Tuning the Band Gap in CsPbBr$_3$ Through Sr Substitution

Daniel B. Straus* and R. J. Cava*

Department of Chemistry, Princeton University, Princeton, NJ 08544 USA

*Authors to whom correspondence should be addressed. Email: dstraus@princeton.edu, rcava@princeton.edu

Abstract

The ability to continuously tune the band gap of a semiconductor allows its optical properties to be precisely tailored for specific applications. We demonstrate that the band gap of the halide perovskite CsPbBr$_3$ can be continuously widened through homovalent substitution of Sr^{2+} for Pb^{2+} using solid-state synthesis, creating a material with the formula CsPb$_{1-x}$Sr$_x$Br$_3$ ($0 \leq x \leq 1$). Sr^{2+} and Pb^{2+} form a solid solution in CsPb$_{1-x}$Sr$_x$Br$_3$. Pure CsPbBr$_3$ has a band gap of 2.29(2) eV, which increases to 2.64(3) eV for CsPb$_{0.25}$Sr$_{0.75}$Br$_3$. Density-functional theory calculations support the hypothesis that Sr incorporation widens the band gap without introducing mid-gap defect states. These results demonstrate that homovalent B-site alloying is a viable method to tune the band gap of halide perovskites without introducing compensating defects that form when B-site cations of a different charge are introduced.

TOC Graphic
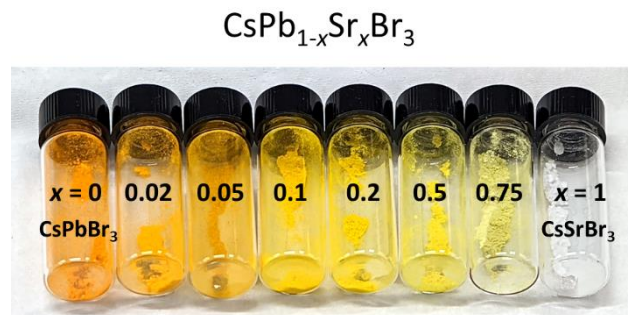
Halide perovskites are best known as semiconductors that have large absorption cross-sections and long carrier diffusion lengths, which allows them to serve as a high-performing active layer in solar cells.[1–6] They typically have the chemical formula ABX$_3$, where A is a 1+ cation, B a 2+ cation, and X a halogen. The relative sizes of the ions restricts the formation of halide perovskites, formalized through the Goldschmidt tolerance factor.[7,8] The band gap of a material is generally determined by the relative electronegativities of its constituents and its electron count, and halide perovskites are no exception.[9–11] Tunable band gaps are desirable because they allow the optical properties of a material to be optimized for a specific application, such as fabricating a light-emitting diode that emits a specific color of light.[12] To tune the band gap of a halide perovskite, a frequently employed method is to change the halogen—chloride-based halide perovskites generally have wider band gaps than bromide-based perovskites, which have wider band gaps than iodide-based perovskites, for example.[13] Incorporating a mixture of halogens allows the band gap to be continuously tuned. Unfortunately, under illumination, phase segregation of the halogens can occur, which lowers the effective band gap of a mixed halide perovskite material to that of one of the end-member perovskites.[13] Incorporating mixtures of A-site cations also allows for limited band gap tunability,[14] but this method is limited in application for all-inorganic lead and tin halide perovskites because Cs$^+$ is the only inorganic cation large enough to stabilize a pure-phase perovskite structure.[15,16]

Another method to tune the band gap is by replacing a fraction of the B-site cations with an alternate cation. This can be accomplished by creating an ordered double perovskite[17] with the formula A$_2$BB'X$_6$ where B is a 1+ and B' a 3+ cation, maintaining an average 2+ charge for the B site.[11,18,19] This is also found for vacancy-ordered halide double perovskites, where for instance B is a 4+ metal and B' is left vacant.[20,21] The most prominent examples of vacancy-ordered double perovskites are members of the A$_2$SnX$_6$ family, where Sn is in the 4+ oxidation state.[22,23] Double perovskites do not allow for continuous band gap tuning— the ratio between B and B' is fixed at 1:1.

The band gap can be tuned by mixing two different 2+ cations on the B-site, but reports of two fully miscible B-site cations in halide perovskites are limited. Lead and tin can be fully mixed in any

concentration on the B-site in halide perovskites, and crystals of this type of material can be grown in solution. Lead and tin halide perovskites have similar band gaps, which limits the overall amount of band gap tunability that perovskites containing lead-tin solid solutions can achieve.[9,24,25]

Other reports have found limited uptake of homovalent B-site cations (*i.e.,* with a 2+ charge) other than tin into a lead halide perovskite, resulting in only weak band gap tuning.[26–31] It was found that when the precursor solutions have a B-site dopant concentration of less than 1 mol percent, then the dopant B-site cation will be incorporated into the parent lead halide perovskite. At higher doping concentrations, however, a secondary phase containing a higher concentration of dopant is formed at the surface.[31] Existing solution-based methods can therefore not be used to widely tune the bandgap of halide perovskites. Heterovalent B-site doping (incorporating B-site cations of a different charge) charge is difficult, and reports of such doping are controversial because incorporating B-site cations that do not have a 2+ charge often results in compensating defect formation elsewhere in the perovskite.[32–34]

Here we show, using solid-state synthesis, that the band gap of the halide perovskite CsPbBr$_3$ can be continuously tuned over hundreds of meV through homovalent B-site doping with strontium. We synthesize the perovskite CsPb$_{1-x}$Sr$_x$Br$_3$ ($0 \leq x \leq 1$) solid solution, where Sr^{2+} and Pb^{2+} are interchangeable and randomly distributed on the B-site. Pb^{2+} and Sr^{2+} have nearly identical ionic radii.[35] CsPbBr$_3$ and CsSrBr$_3$ are both known. CsSrBr$_3$ is a wide-band gap white orthorhombic halide perovskite that is used as a scintillator when doped with rare earth ions.[36,37] Compared to the 2.29(2) eV band gap of pure CsPbBr$_3$, replacing 75% of the Pb^{2+} cations with Sr^{2+} increases the band gap by 350 meV to 2.64(3) eV. Pure phase CsSrBr$_3$ has a band gap beyond the visible regime, so it is colorless because it does not significantly absorb visible light. Density functional theory calculations support the observation that replacing Pb^{2+} with Sr^{2+} increases the band gap, consistent with the relative electronegativities of Sr^{2+} and Pb^{2+}. These results demonstrate that homovalent B-site alloying is a viable strategy to continuously tune the band gap of halide perovskites, which may enable optical applications where it is necessary to dial in the precise band gap of a material.[36]

Figure 1 shows the powder X-ray diffraction patterns for CsPbBr$_3$ and CsSrBr$_3$. All the observed reflections index to reported orthorhombic unit cells.[38,39] The reported lattice constants of CsPbBr$_3$ and CsSrBr$_3$ differ from one another by less than 1%, consistent with the nearly identical ionic radii of six-coordinate Pb^{2+} and Sr^{2+}, which only differ by 0.01Å in Shannon's table.[35] The powder diffraction patterns for CsPb$_{1-x}$Sr$_x$Br$_3$ are shown in Figure 1, and like pure-phase CsPbBr$_3$ and CsSrBr$_3$ they are all orthorhombic perovskites with no obvious differences in their patterns compared to the patterns of pure-phase CsPbBr$_3$ and CsSrBr$_3$. Importantly, the mixed Pb-Sr species do not exhibit any superlattice reflections when compared to CsPbBr$_3$ and CsSrBr$_3$, indicating that Pb^{2+} and Sr^{2+} do not order within the perovskite structure even for a 1:1 mixture of Sr and Br (CsPb$_{0.5}$Sr$_{0.5}$Br$_3$, x =0.5). Instead, Pb^{2+} and Sr^{2+} form a solid solution where they are randomly distributed among B-sites, like what was found in mixed lead-tin halide perovskites.[24] Because Sr^{2+} and Pb^{2+} have the same charge and are approximately the same size, any driving force toward ordering would have to involve the difference in their relative electronegativites, which is apparently not sufficient. In contrast, other reported mixed cation halide perovskites such as Cs$_2$AgBiBr$_3$ form double perovskites, where Ag$^+$ and In^{3+} are ordered within the crystal and occupy adjacent B-sites.[11,18,40] Thus, B site order in heterovalent double perovskite halides appears to be promoted by the distinct charges of each of the two cations.
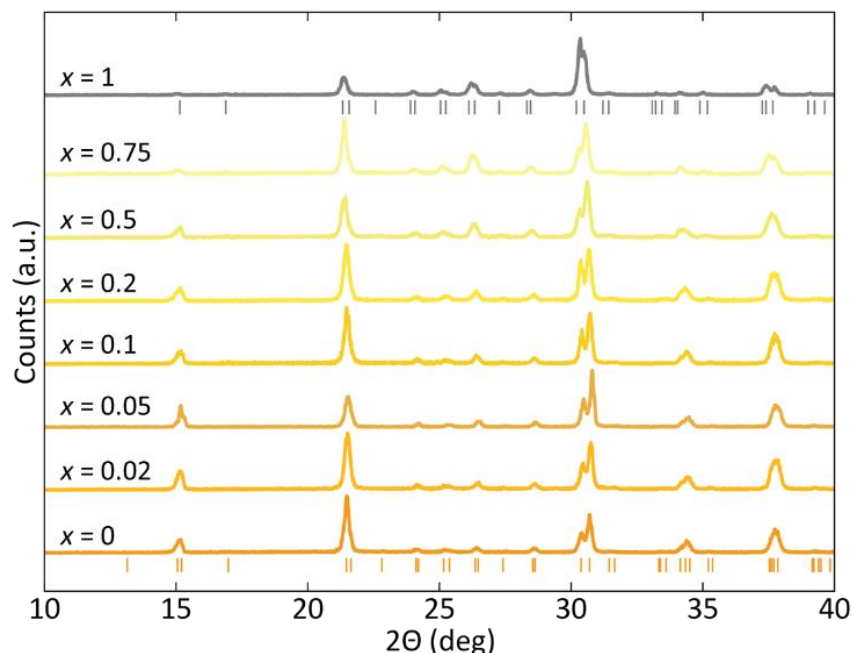
Figure 1: Structural characterization. Powder X-ray diffraction patterns of CsPb$_{1-x}$Sr$_x$Br$_3$ (x = 0-1). Locations of reflections for CsPbBr$_3$ and CsSrBr$_3$ from previously reported patterns are indicated by orange and grey bars, respectively.

Figure 2a shows ground powders as well as intact pieces of CsPb$_{1-x}$Sr$_x$Br$_3$ (x = 0, 0.02, 0.05, 0.1, 0.2, 0.5, 0.75 and 1) inside a nitrogen-filled glove box. Pseudoabsorbance spectra are shown in Figure 2b, with extracted band gaps in Figure 2c. CsPbBr$_3$ is a bright orange solid with a band gap of 2.29(2) eV, matching what has been previously reported.[15] As the concentration of Sr^{2+} increases, the color of the material becomes a lighter orange and then a light yellow, reaching a band gap of 2.64(3) eV for x = 0.75, which is 350 meV larger than that of pure-phase CsPbBr$_3$. Pure-phase CsSrBr$_3$ is a wide band gap semiconductor that is white in color, consistent with its absorption spectrum which suggests it has an optical band gap exceeding 3.5 eV (Figure 2b). CsSrBr$_3$ has been explored as a scintillator for X-ray detection when doped with 2+ rare earth cations such as Eu^{2+}.[36,37]
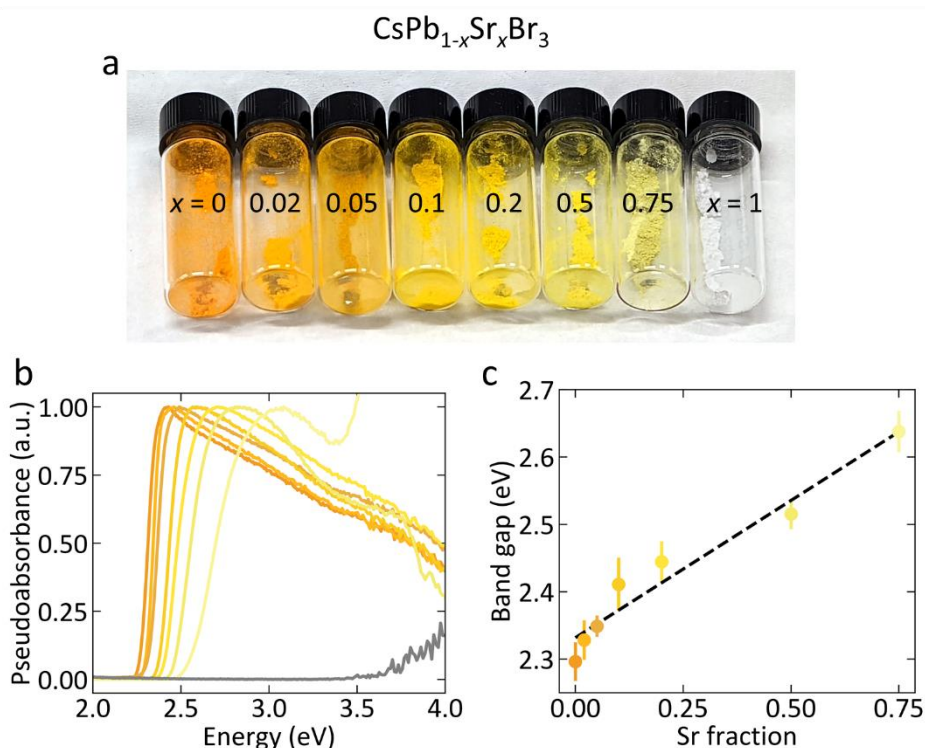
Figure 2: Optical characterization. (a) Photograph of ground powders and intact pieces of CsPb$_{1-x}$Sr$_x$Br$_3$ with x indicated on corresponding vial. (b) Pseudoabsorption spectra and (c) extracted band gaps for CsSr$_x$Pb$_{1-x}$Br$_3$ with a linear regression ($R^2 = 0.95$) shown in black. The color of each trace in (b) and point in (c) is set to the color of the material in (a), with pure CsSrBr$_3$ shown in grey.

It was previously reported that the band gap of the orange-colored halide perovskite CsPbBr$_3$ could be continuously reduced through heterovalent doping. In that case, a small amount of Bi^{3+} was said to replace Pb^{2+}. Crystals incorporating Bi^{3+} became much darker than those of pure CsPbBr$_3$.[32] However, later studies showed that the intrinsic band gap was not changed through Bi^{3+} incorporation and instead compensating defects were formed in the crystal to offset the excess charge of the Bi^{3+} cation. This process creates localized states that absorb a small fraction of sub band-gap light.[33,34] The increased band gap reported here from Sr^{2+} incorporation caused by the formation of localized defects. Mid-gap defects can only *decrease* the apparent band gap of the material, whereas the band gap of CsPb$_{1-x}$Sr$_x$Br$_3$ increases with Sr^{2+} content. The bulk electronic structure of the perovskite is therefore changed through strontium incorporation.
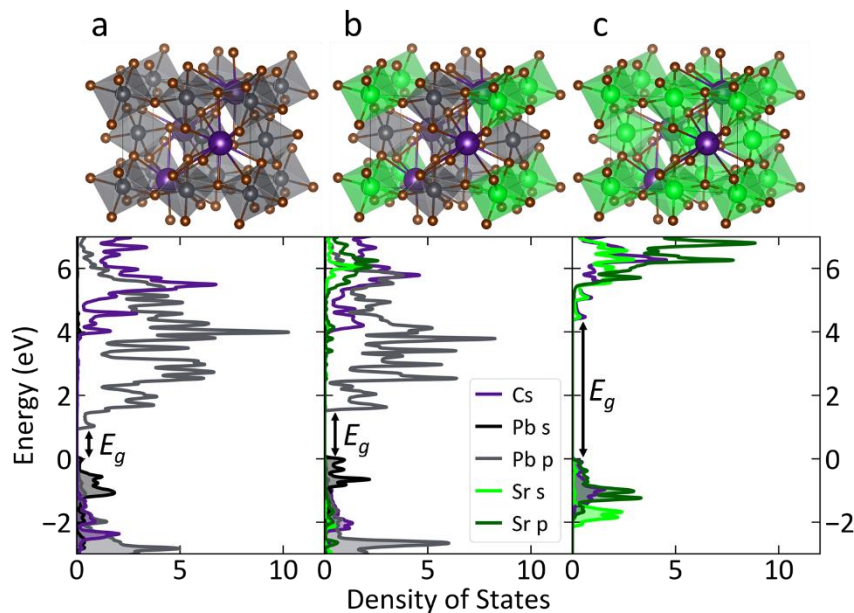
Figure 3: Results of the electronic structure calculations. Relaxed structures used to compute projected density of states (top), with Cs depicted in purple, Pb in grey, Sr in green, and Br in brown, and computed projected density of states (bottom) for (a) CsPbBr$_3$, (b) CsSr$_{0.25}$Pb$_{0.75}$Br$_3$, and (c) CsSrBr$_3$, with (black arrow) band gap E_g. The Fermi energy set to 0 eV in all panels.

Density-functional theory calculations support our observation that Sr^{2+} substitution for Pb^{2+} in CsPbBr$_3$ increases the band gap. Figure 3a shows the projected density of states of the Cs and Pb atoms in CsPbBr$_3$. In line with previous computations for CsPbBr$_3$ and other lead halide perovskites,[41,42] the top of the valence band is predominantly composed of halide *p* orbitals with some contribution from Pb *s* orbitals, and the bottom of the conduction band is mostly Pb *p* in character. CsPbBr$_3$ has a computed band gap of 1.00 eV, which is much smaller than the experimental value. DFT calculations are known to dramatically underestimate the band gap of lead halide perovskites,[43] and our computed band gap is consistent with earlier calculations that like our calculations account for spin-orbit coupling.[44]

Replacing the Pb atom at (0,0,0) with Sr results in the model compound CsSr$_{0.25}$Pb$_{0.75}$Br$_3$, and the projected density of states of the Cs, Pb, and Sr atoms is shown in Figure 3b. CsSr$_{0.25}$Pb$_{0.75}$Br$_3$ has a computed band gap of 1.53 eV, 0.53 eV larger than that of CsPbBr$_3$. Like in pure CsPbBr$_3$, the top of the valence band is predominantly composed of halide *p* orbitals with some contribution from Pb *s* orbitals, and the bottom of the conduction band is predominantly Pb *p* in character. There is negligible contribution

of Sr orbitals near the top of the valence band or the bottom of the conduction band, but the presence of Sr in the material opens the band gap. Sr incorporation does not introduce any mid-gap states. This computational result is consistent with an earlier result that showed the computed band gap of the hybrid perovskite methylammonium lead iodide increased with 25% Ba^{2+} substitution for Pb^{2+}.[27] We note that the structural model that we used for the computation of the electronic structure of $CsSr_{0.25}Pb_{0.75}Br_3$ contains a Pb-Sr superlattice because the Sr atom is located at a single well-defined crystallographic position. More sophisticated random site occupancy models for the doped material may be of interest in future calculations. Figure 3c shows the projected density of states of the Cs and Sr atoms in $CsSrBr_3$, which has a much larger computed band gap of 4.45 eV (Figure 3c), consistent with its wider experimental band gap.

Upon exposure to atmosphere, $CsPb_{1-x}Sr_xBr_3$ ($x \neq 1$) rapidly turns orange. Pseudoabsorbance spectra of air-exposed $CsPb_{1-x}Sr_xBr_3$ are shown in Figure 4a. The band gaps of the air-exposed materials are statistically indistinguishable from that of pure $CsPbBr_3$ (Figure 4b). Pure $CsSrBr_3$ is deliquescent and rapidly dissolves itself when taken out of inert atmosphere. X-ray diffraction patterns of air-exposed $CsPb_{1-x}Sr_xBr_3$ ($x \neq 1$) are shown in Figure 4c. The diffraction patterns demonstrate that the orange color upon exposure to air is caused by the decomposition of $CsPb_{1-x}Sr_xBr_3$ ($x \neq 1$) into $CsPbBr_3$. Two other phases are also present and are especially evident in the $x = 0.5$ and 0.75 samples: Cs_4PbBr_6 (red, Figure 4c) and $SrBr_2 \cdot H_2O$ (blue, Figure 4c);[45,46] an additional unidentified phase containing Pb must also be present to account for all atoms. The hump in the absorption spectrum centered around 2.7 eV in $CsPb_{1-x}Sr_xBr_3$ ($x = 0.5$ and 0.75) is consistent with the presence of Cs_4PbBr_6, which has a band gap of 2.37 eV.[47] There is also a strong absorption feature beginning around 3.6 eV in the air-exposed $CsPb_{1-x}Sr_xBr_3$ ($x = 0.5$ and 0.75) materials, and we do not know what material causes it. Further study is needed to understand how and why exposure to air causes Sr^{2+} to come out of the perovskite lattice, leaving pure $CsPbBr_3$ behind in addition to other byproducts. We hypothesize that the degradation mechanism is likely similar to the still-unknown mechanism by which metastable black perovskite-phase $CsPbI_3$ is converted to a non-perovskite yellow phase when exposed to moisture.[48]
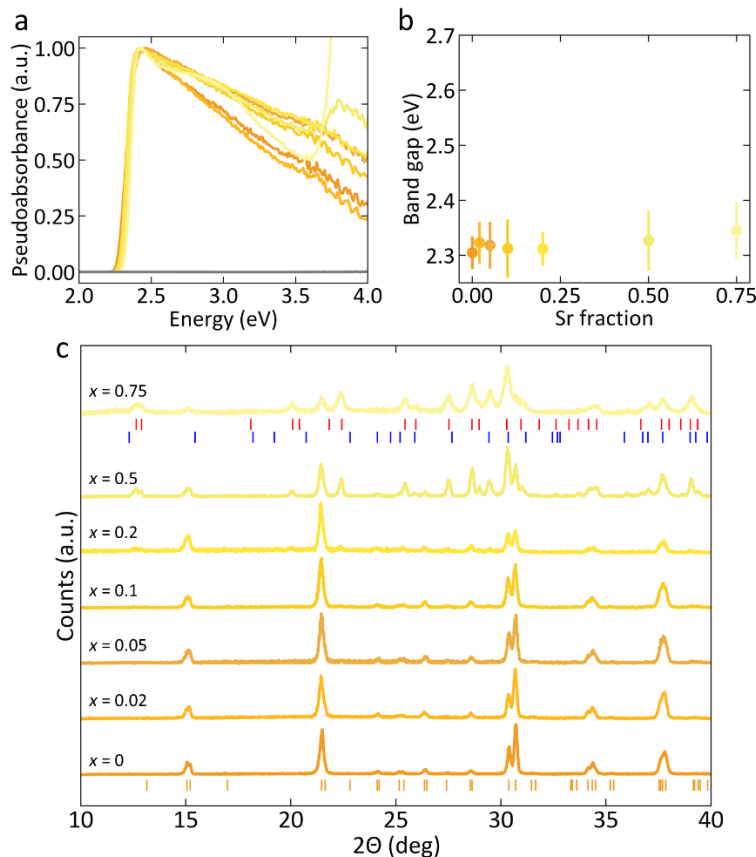
Figure 4: Sample degradation in air. (a) Pseudoabsorption spectra, (b) optical band gaps, and (c) powder X-ray diffraction patterns of air-exposed CsPb$_{1-x}$Sr$_x$Br$_3$, with indexed reflections for CsPbBr$_3$, Cs$_2$PbBr$_6$, and SrBr$_2$·H$_2$O shown in orange, red, and blue, respectively.

We demonstrate that B-site alloying is a viable method to tune the band gap in halide perovskites by synthesizing and characterizing CsPb$_{1-x}$Sr$_x$Br$_3$ ($x = 0 - 1$). While most solution-based syntheses limit the amount of B-site dopant that can be incorporated into the perovskite lattice, solid-state synthesis removes this limitation. In CsPbBr$_3$, we replace up to 75% of Pb^{2+} with Sr^{2+}, allowing the band gap to be continuously increased from 2.29(2) eV for pure CsPbBr$_3$ to 2.64(3) eV for CsPb$_{0.25}$Sr$_{0.75}$Br$_3$. Sr^{2+} and Pb^{2+} form a solid solution in CsPb$_{1-x}$Sr$_x$Br$_3$ where they are randomly distributed throughout the lattice. The identical charge and similar size of Pb^{2+} and Sr^{2+} does not allow them to spontaneously segregate onto distinct lattice sites, unlike in charge-ordered or vacancy-ordered double perovskites. DFT calculations support the widening of the band gap of CsPbBr$_3$ upon Sr^{2+} substitution. In the future, it may be possible to develop solution-

compatible processes that will allow for the ambient temperature incorporation of large amounts of homovalent B-site dopants to provide another route to tune halide perovskite band gaps for optical applications.[36]

Experimental

SrBr$_2$ (Alfa Aesar, 99%, anhydrous) was dried overnight under rough vacuum at 230 °C. It was then brought into an argon-filled glove box, loaded into a quartz tube, transferred to an ampoule sealing line, and evacuated to high vacuum. While under high vacuum, the SrBr$_2$ was melted with a methane-oxygen torch to assist in removing residual moisture. Black impurities formed that were not soluble in molten SrBr$_2$. The quartz tube was refilled with argon, a graphite piece was added to the top of the tube to aid in removing residual moisture, and the tube was evacuated to high vacuum (10^{-4} torr) and then sealed. The ampoule was heated at 700 °C in a furnace, cooled to room temperature at 30 °C/hr, and opened in an argon-filled glove box. The solidified melt containing the black impurities was loaded in a new quartz ampoule with quartz wool placed above the impure SrBr$_2$ to act as a filter in hot centrifugation. The tube was evacuated and sealed under high vacuum, and the ampoule was then heated to 900 °C in a furnace. It was removed from the furnace while hot, inverted, and centrifuged. The quartz wool trapped the black impurities, allowing the molten SrBr$_2$ to pass to the other end of the ampoule, where it solidified into a very light gray lump. The ampoule was opened in an argon-filled glove box, and the purified SrBr2 was ground into a white powder.

CsPb$_{1-x}$Sr$_x$Br$_3$ (x = 0, 0.02, 0.05, 0.1, 0.2, 0.5, 0.75 and 1) was synthesized by weighing out stoichiometric amounts of CsBr (Sigma-Aldrich, 99.999%, anhydrous), SrBr$_2$ (purified as described above), and PbBr$_2$ (Alfa Aesar, 99.999%, ultra dry) in an argon-filled glove box and placing the reagents in quartz tubes. The quartz tubes were sealed under vacuum (10^{-3} torr), and the ampoules were heated to 810 °C in a furnace, melting the reagents. The ampoules were subsequently cooled to room temperature, at which point they were brought into a nitrogen-filled glove box, opened, and the melt ground in a mortar.

Powder X-ray diffraction patterns were taken on a Rigaku Miniflex II diffractometer that was located inside a nitrogen-filled glove box, using Cu kα radiation (λ = 1.5406Å). Diffuse reflectance spectra were taken on an Agilent Cary 5000 UV-Vis-NIR spectrometer equipped with an Agilent DRA-2500 internal diffuse reflectance accessory. For the diffuse reflectance measurements, $CsPb_{1-x}Sr_xBr_3$ was diluted to approximately 10% w/w with dry MgO and placed in Agilent powder sample holders that were sealed with an O-ring. Diffuse reflectance spectra were converted to pseudoabsorbance spectra using the Kubelka-Munk function.[49] Band gaps were calculated using the direct band gap Tauc model.[50]

Density-functional theory calculations were performed with Quantum Espresso[51,52] version 6.8 using the generalized gradient approximation functionals by Perdew, Burke, and Ernzerhof[53] and PSLibrary v1.0.0 pseudopotentials.[54] The starting structure of CsPbBr$_3$ employed was the crystal structure published in Ref. [15] accessed through the Inorganic Crystal Structure Database[55] (ICSD Collection Code 243735). The initial structure of CsSrBr$_3$ was generated by replacing the Pb atoms in the CsPbBr$_3$ structure with Sr. The initial structure of $CsSr_{0.25}Pb_{0.75}Br_3$ was generated by converting the orthorhombic CsPbBr$_3$ structure to triclinic P-1 and replacing the Pb atom at (0,0,0) with Sr. The coordinates of all structures were optimized using the *vc-relax* routine in a scalar relativistic calculation, and the scalar relativistic-optimized structures were then optimized once more using a fully relativistic calculation. An automatically generated 5x5x5 unshifted *k*-point mesh was used for structural relaxation. The density of states was calculated using an automatically generated 10x10x10 unshifted *k*-point mesh in a fully relativistic calculation that accounts for spin-orbit coupling effects. The kinetic energy cutoff for wavefunctions was set to 60 Ry, and the kinetic energy cutoff for charge density and potential was set to 300 Ry for all calculations. The total energy convergence threshold was set to 10^{-8}, the force convergence threshold was set to 10^{-5}, and the self-consistency convergence threshold was set to 10^{-8}. 50 meV of Gaussian broadening was used when generating the projected density of states.

References:

(1)   Dong, Q.; Fang, Y.; Shao, Y.; Mulligan, P.; Qiu, J.; Cao, L.; Huang, J. Electron-Hole Diffusion
        Lengths > 175 Um in Solution-Grown CH 3 NH 3 PbI 3 Single Crystals. *Science* **2015**, *347*, 967–
        970.

(2)   Semonin, O. E.; Elbaz, G. A.; Straus, D. B.; Hull, T. D.; Paley, D. W.; van der Zande, A. M.;
        Hone, J. C.; Kymissis, I.; Kagan, C. R.; Roy, X.; Owen, J. S. Limits of Carrier Diffusion in n -
        Type and p -Type CH 3 NH 3 PbI 3 Perovskite Single Crystals. *J. Phys. Chem. Lett.* **2016**, *7*,
        3510–3518.

(3)   Bi, Y.; Hutter, E. M.; Fang, Y.; Dong, Q.; Huang, J.; Savenije, T. J. Charge Carrier Lifetimes
        Exceeding 15 Ms in Methylammonium Lead Iodide Single Crystals. *J. Phys. Chem. Lett.* **2016**, *7*,
        923–928.

(4)   Zhu, X.-Y.; Podzorov, V. Charge Carriers in Hybrid-Organic–Inorganic Lead-Halide Perovskites
        Might Be Protected as Large Polarons. *J. Phys. Chem. Lett.* **2015**, *6*, 4758–4761.

(5)   Green, M. A.; Ho-Baillie, A.; Snaith, H. J. The Emergence of Perovskite Solar Cells. *Nat.
        Photonics* **2014**, *8*, 506–514.

(6)   NREL. Best Research-Cell Efficiencies http://www.nrel.gov/pv/assets/images/efficiency-chart.png
        (accessed Jan 27, 2022).

(7)   Filip, M. R.; Giustino, F. The Geometric Blueprint of Perovskites. *Proc. Natl. Acad. Sci.* **2018**,
        115, 5397–5402.

(8)   Goldschmidt, V. M. Die Gesetze Der Krystallochemie. *Naturwissenschaften* **1926**, *14*, 477–485.

(9)   Jena, A. K.; Kulkarni, A.; Miyasaka, T. Halide Perovskite Photovoltaics: Background, Status, and
        Future Prospects. *Chem. Rev.* **2019**, *119*, 3036–3103.

(10)   Hoffmann, R. How Chemistry and Physics Meet in the Solid State. *Angew. Chemie Int. Ed.
        English* **1987**, *26*, 846–878.

(11)   Slavney, A. H.; Connor, B. A.; Leppert, L.; Karunadasa, H. I. A Pencil-and-Paper Method for
        Elucidating Halide Double Perovskite Band Structures. *Chem. Sci.* **2019**, *10*, 11041–11053.

(12)   Adjokatse, S.; Fang, H. H.; Loi, M. A. Broadly Tunable Metal Halide Perovskites for Solid-State
        Light-Emission Applications. *Mater. Today* **2017**, *20*, 413–424.

(13)   Hoke, E. T.; Slotcavage, D. J.; Dohner, E. R.; Bowring, A. R.; Karunadasa, H. I.; McGehee, M. D.
        Reversible Photo-Induced Trap Formation in Mixed-Halide Hybrid Perovskites for Photovoltaics.
        Chem. Sci. **2015**, *6*, 613–617.

(14) McMeekin, D. P.; Sadoughi, G.; Rehman, W.; Eperon, G. E.; Saliba, M.; Hörantner, M. T.; Haghighirad, A.; Sakai, N.; Korte, L.; Rech, B.; Johnston, M. B.; Herz, L. M.; Snaith, H. J. A Mixed-Cation Lead Mixed-Halide Perovskite Absorber for Tandem Solar Cells. *Science* **2016**, *351*, 151–155.

(15) Linaburg, M. R.; McClure, E. T.; Majher, J. D.; Woodward, P. M. Cs1-XRbxPbCl3 and Cs1-XRbxPbBr3 Solid Solutions: Understanding Octahedral Tilting in Lead Halide Perovskites. *Chem. Mater.* **2017**, *29*, 3507–3514.

(16) Straus, D. B.; Guo, S.; Abeykoon, A. M.; Cava, R. J. Understanding the Instability of the Halide Perovskite CsPbI 3 through Temperature-Dependent Structural Analysis. *Adv. Mater.* **2020**, *32*, 2001069.

(17) Anderson, M. T.; Greenwood, K. B.; Taylor, G. A.; Poeppelmeier, K. R. B-Cation Arrangements in Double Perovskites. *Prog. Solid State Chem.* **1993**, *22*, 197–233.

(18) Slavney, A. H.; Hu, T.; Lindenberg, A. M.; Karunadasa, H. I. A Bismuth-Halide Double Perovskite with Long Carrier Recombination Lifetime for Photovoltaic Applications. *J. Am. Chem. Soc.* **2016**, *138*, 2138–2141.

(19) Slavney, A. H.; Leppert, L.; Saldivar Valdes, A.; Bartesaghi, D.; Savenije, T. J.; Neaton, J. B.; Karunadasa, H. I. Small-Band-Gap Halide Double Perovskites. *Angew. Chemie - Int. Ed.* **2018**, *57*, 12765–12770.

(20) Maughan, A. E.; Ganose, A. M.; Scanlon, D. O.; Neilson, J. R. Perspectives and Design Principles of Vacancy-Ordered Double Perovskite Halide Semiconductors. *Chem. Mater.* **2019**, *31*, 1184–1195.

(21) Brik, M. G.; Kityk, I. V. Modeling of Lattice Constant and Their Relations with Ionic Radii and Electronegativity of Constituting Ions of A2XY6 Cubic Crystals (A=K, Cs, Rb, Tl; X=tetravalent Cation, Y=F, Cl, Br, I). *J. Phys. Chem. Solids* **2011**, *72*, 1256–1260.

(22) Lee, B.; Stoumpos, C. C.; Zhou, N.; Hao, F.; Malliakas, C.; Yeh, C. Y.; Marks, T. J.; Kanatzidis, M. G.; Chang, R. P. H. Air-Stable Molecular Semiconducting Iodosalts for Solar Cell Applications: Cs2SnI6 as a Hole Conductor. *J. Am. Chem. Soc.* **2014**, *136*, 15379–15385.

(23) Maughan, A. E.; Ganose, A. M.; Candia, A. M.; Granger, J. T.; Scanlon, D. O.; Neilson, J. R. Anharmonicity and Octahedral Tilting in Hybrid Vacancy-Ordered Double Perovskites. *Chem. Mater.* **2018**, *30*, 472–483.

(24) Hao, F.; Stoumpos, C. C.; Chang, R. P. H.; Kanatzidis, M. G. Anomalous Band Gap Behavior in Mixed Sn and Pb Perovskites Enables Broadening of Absorption Spectrum in Solar Cells. *J. Am. Chem. Soc.* **2014**, *136*, 8094–8099.

(25) Zhao, B.; Abdi-Jalebi, M.; Tabachnyk, M.; Glass, H.; Kamboj, V. S.; Nie, W.; Pearson, A. J.; Puttisong, Y.; Gödel, K. C.; Beere, H. E.; Ritchie, D. A.; Mohite, A. D.; Dutton, S. E.; Friend, R. H.; Sadhanala, A. High Open-Circuit Voltages in Tin-Rich Low-Bandgap Perovskite-Based Planar Heterojunction Photovoltaics. *Adv. Mater.* **2017**, *29*.

(26) Pérez-del-Rey, D.; Forgács, D.; Hutter, E. M.; Savenije, T. J.; Nordlund, D.; Schulz, P.; Berry, J. J.; Sessolo, M.; Bolink, H. J. Strontium Insertion in Methylammonium Lead Iodide: Long Charge

Carrier Lifetime and High Fill-Factor Solar Cells. *Adv. Mater.* **2016**, *28*, 9839–9845.

(27)   Zhang, H.; Shang, M. hui; Zheng, X.; Zeng, Z.; Chen, R.; Zhang, Y.; Zhang, J.; Zhu, Y. Ba2+ Doped CH3NH3PbI3 to Tune the Energy State and Improve the Performance of Perovskite Solar Cells. *Electrochim. Acta* **2017**, *254*, 165–171.

(28)   Mondal, A.; Lata, A.; Gupta, S. Effect of Sr2+ Doping on Optical, Thermal and Photocatalytic Behaviour of CsPbBr3. *Mater. Lett.* **2021**, No. November, 131314.

(29)   Karunakaran, S. K.; Arumugam, G. M.; Yang, W.; Ge, S.; Khan, S. N.; Mai, Y.; Lin, X.; Yang, G. Europium (II)-Doped All-Inorganic CsPbBr3 Perovskite Solar Cells with Carbon Electrodes. *Sol. RRL* **2020**, *2000390*, 1–8.

(30)   Zhao, Y.; Wang, Y.; Duan, J.; Yang, X.; Tang, Q. Divalent Hard Lewis Acid Doped CsPbBr 3 Films for 9.63%-Efficiency and Ultra-Stable All-Inorganic Perovskite Solar Cells. *J. Mater. Chem. A* **2019**, *7*, 6877–6882.

(31)   Phung, N.; Félix, R.; Meggiolaro, D.; Al-Ashouri, A.; Sousa e Silva, G.; Hartmann, C.; Hidalgo, J.; Köbler, H.; Mosconi, E.; Lai, B.; Gunder, R.; Li, M.; Wang, K.-L.; Wang, Z.-K.; Nie, K.; Handick, E.; Wilks, R. G.; Marquez, J. A.; Rech, B.; Unold, T.; Correa-Baena, J.-P.; Albrecht, S.; De Angelis, F.; Bär, M.; Abate, A. The Doping Mechanism of Halide Perovskite Unveiled by Alkaline Earth Metals. *J. Am. Chem. Soc.* **2020**, *142*, 2364–2374.

(32)   Abdelhady, A. L.; Saidaminov, M. I.; Murali, B.; Adinolfi, V.; Voznyy, O.; Katsiev, K.; Alarousu, E.; Comin, R.; Dursun, I.; Sinatra, L.; Sargent, E. H.; Mohammed, O. F.; Bakr, O. M. Heterovalent Dopant Incorporation for Bandgap and Type Engineering of Perovskite Crystals. *J. Phys. Chem. Lett.* **2016**, *7*, 295–301.

(33)   Nayak, P. K.; Sendner, M.; Wenger, B.; Wang, Z.; Sharma, K.; Ramadan, A. J.; Lovrinčić, R.; Pucci, A.; Madhu, P. K.; Snaith, H. J. Impact of Bi3+ Heterovalent Doping in Organic-Inorganic Metal Halide Perovskite Crystals. *J. Am. Chem. Soc.* **2018**, *140*, 574–577.

(34)   Lozhkina, O. A.; Murashkina, A. A.; Shilovskikh, V. V.; Kapitonov, Y. V.; Ryabchuk, V. K.; Emeline, A. V.; Miyasaka, T. Invalidity of Band-Gap Engineering Concept for Bi3+ Heterovalent Doping in CsPbBr3 Halide Perovskite. *J. Phys. Chem. Lett.* **2018**, *9*, 5408–5411.

(35)   Shannon, R. D. Revised Effective Ionic Radii and Systematic Studies of Interatomic Distances in Halides and Chalcogenides. *Acta Crystallogr. Sect. A* **1976**, *32*, 751–767.

(36)   Gokhale, S. S.; Stand, L.; Lindsey, A.; Koschan, M.; Zhuravleva, M.; Melcher, C. L. Improvement in the Optical Quality and Energy Resolution of CsSrBr3: Eu Scintillator Crystals. *J. Cryst. Growth* **2016**, *445*, 1–8.

(37)   Suta, M.; Larsen, P.; Lavoie-Cardinal, F.; Wickleder, C. Photoluminescence of CsMBr3:Eu2+ (M=Mg, Ca, Sr) - A Novel Strategy for the Development of Low-Energy Emitting Phosphors. *J. Lumin.* **2014**, *149*, 35–44.

(38)   Rodová, M.; Brožek, J.; Knížek, K.; Nitsch, K. Phase Transitions in Ternary Caesium Lead Bromide. *J. Therm. Anal. Calorim.* **2003**, *71*, 667–673.

(39)   Meyer, G.; Schilling, G. CsSrBr3 PDF 00-044-1375. *ICDD Grant-in-Aid*. Inst. Anorganische

Chemie, Univ. Hannover: Hannover, Germany 1993.

(40)   McClure, E. T.; Ball, M. R.; Windl, W.; Woodward, P. M. Cs 2 AgBiX 6 (X = Br, Cl): New Visible Light Absorbing, Lead-Free Halide Perovskite Semiconductors. *Chem. Mater.* **2016**, *28*, 1348–1354.

(41)   Yin, W. J.; Shi, T.; Yan, Y. Unique Properties of Halide Perovskites as Possible Origins of the Superior Solar Cell Performance. *Adv. Mater.* **2014**, *26*, 4653–4658.

(42)   Manser, J. S.; Christians, J. A.; Kamat, P. V. Intriguing Optoelectronic Properties of Metal Halide Perovskites. *Chem. Rev.* **2016**, *116*, 12956–13008.

(43)   Perdew, J. P. Density Functional Theory and the Band Gap Problem. *Int. J. Quantum Chem.* **2009**, *28*, 497–523.

(44)   Ghaithan, H. M.; Alahmed, Z. A.; Qaid, S. M. H.; Hezam, M.; Aldwayyan, A. S. Density Functional Study of Cubic, Tetragonal, and Orthorhombic CsPbBr 3 Perovskite. *ACS Omega* **2020**, *5*, 7468–7480.

(45)   Engelen, B.; Freiburg, C.; Lutz, H. D. Zur Kenntnis Der Hydrate Des Typs MX 2 · 1 H 2 O Mit M = Sr, Ba Und X = Cl, Br, I. Kristallstrukturen Des Strontiumchlorid-Monohydrats, SrCl 2 · 1 H 2 O, Und Des Strontiumbromid-Monohydrats, SrBr 2 · 1 H 2 O. *Zeitschrift für Anorg. und Allg. Chemie* **1983**, *497*, 151–156.

(46)   Velázquez, M.; Ferrier, A.; Péchev, S.; Gravereau, P.; Chaminade, J.-P.; Portier, X.; Moncorgé, R. Growth and Characterization of Pure and Pr3+-Doped Cs4PbBr6 Crystals. *J. Cryst. Growth* **2008**, *310*, 5458–5463.

(47)   Andrews, R. H.; Clark, S. J.; Donaldson, J. D.; Dewan, J. C.; Silver, J. Solid-State Properties of Materials of the Type Cs4MX6(Where M = Sn or Pb and X = Cl or Br). *J. Chem. Soc. Dalt. Trans.* **1983**, No. 4, 767.

(48)   Straus, D. B.; Guo, S.; Cava, R. J. Kinetically Stable Single Crystals of Perovskite-Phase CsPbI 3. *J. Am. Chem. Soc.* **2019**, *141*, 11435–11439.

(49)   Hecht, H. G. The Interpretation of Diffuse Reflectance Spectra. *J. Res. Natl. Bur. Stand. Sect. A Phys. Chem.* **1976**, *80A*, 567.

(50)   Viezbicke, B. D.; Patel, S.; Davis, B. E.; Birnie, D. P. Evaluation of the Tauc Method for Optical Absorption Edge Determination: ZnO Thin Films as a Model System. *Phys. status solidi* **2015**, *252*, 1700–1710.

(51)   Giannozzi, P.; Baroni, S.; Bonini, N.; Calandra, M.; Car, R.; Cavazzoni, C.; Ceresoli, D.; Chiarotti, G. L.; Cococcioni, M.; Dabo, I.; Dal Corso, A.; de Gironcoli, S.; Fabris, S.; Fratesi, G.; Gebauer, R.; Gerstmann, U.; Gougoussis, C.; Kokalj, A.; Lazzeri, M.; Martin-Samos, L.; Marzari, N.; Mauri, F.; Mazzarello, R.; Paolini, S.; Pasquarello, A.; Paulatto, L.; Sbraccia, C.; Scandolo, S.; Sclauzero, G.; Seitsonen, A. P.; Smogunov, A.; Umari, P.; Wentzcovitch, R. M. QUANTUM ESPRESSO: A Modular and Open-Source Software Project for Quantum Simulations of Materials. *J. Phys. Condens. Matter* **2009**, *21*, 395502.

(52)   Giannozzi, P.; Andreussi, O.; Brumme, T.; Bunau, O.; Nardelli, M. B.; Calandra, M.; Car, R.;

Cavazzoni, C.; Ceresoli, D.; Cococcioni, M.; others. Advanced Capabilities for Materials Modelling with Quantum ESPRESSO. (ArXiv:1709.10010v1 [Cond-Mat.Mtrl-Sci]). *J. Phys. Condens. Matter* **2017**, *29*, 465901.

(53)   Perdew, J. P.; Burke, K.; Ernzerhof, M. Generalized Gradient Approximation Made Simple. *Phys. Rev. Lett.* **1996**, *77*, 3865–3868.

(54)   Dal Corso, A. Pseudopotentials Periodic Table: From H to Pu. *Comput. Mater. Sci.* **2014**, *95*, 337–350.

(55)   Hellenbrandt, M. The Inorganic Crystal Structure Database (ICSD) - Present and Future. In *Crystallography Reviews*; 2004; Vol. 10, pp 17–22.